Regulation of T7 gp2.5 binding dynamics by its C-terminal tail, template conformation and sequence

Xu, Longfu; Cabanas-Danes, Jordi; Halma, Matthew T.J.; Heller, Iddo; Stratmann, Sarah A.; Van Oijen, Antoine M.; Lee, Seung Joo; Peterman, Erwin J. G.; Wuite, Gijs J. L.

Published in:
Nucleic Acids Research

DOI:
10.1093/nar/gkad485

Publication date:
2023

6540–6553 *Nucleic Acids Research, 2023, Vol. 51, No. 13* *Published online 31 May 2023*
https://doi.org/10.1093/nar/gkad485

Regulation of T7 gp2.5 binding dynamics by its C-terminal tail, template conformation and sequence

Longfu Xu [1,†], Jordi Cabanas-Danés [1,†], Matthew T.J. Halma [1,†], Iddo Heller[1], Sarah A. Stratmann[2], Antoine M. van Oijen[3], Seung-Joo Lee[4], Erwin J.G. Peterman[1] and Gijs J.L. Wuite[1,*]

[1]Department of Physics and Astronomy, Vrije Universiteit Amsterdam, De Boelelaan 1081, 1081 HV, Amsterdam, The Netherlands, [2]Zernike Institute for Advanced Materials, University of Groningen, Groningen 9747 AG, The Netherlands, [3]Molecular Horizons and School of Chemistry and Molecular Bioscience, University of Wollongong, and Illawarra Health and Medical Research Institute, Wollongong, NSW 2522, Australia and [4]Department of Biological Chemistry and Molecular Pharmacology, Harvard Medical School, Boston, MA, USA

Received July 29, 2022; Revised April 27, 2023; Editorial Decision April 28, 2023; Accepted May 19, 2023

ABSTRACT

Bacteriophage T7 single-stranded DNA-binding protein (gp2.5) binds to and protects transiently exposed regions of single-stranded DNA (ssDNA) while dynamically interacting with other proteins of the replication complex. We directly visualize fluorescently labelled T7 gp2.5 binding to ssDNA at the single-molecule level. Upon binding, T7 gp2.5 reduces the contour length of ssDNA by stacking nucleotides in a force-dependent manner, suggesting T7 gp2.5 suppresses the formation of secondary structure. Next, we investigate the binding dynamics of T7 gp2.5 and a deletion mutant lacking 21 C-terminal residues (gp2.5-Δ21C) under various template tensions. Our results show that the base sequence of the DNA molecule, ssDNA conformation induced by template tension, and the acidic terminal domain from T7 gp2.5 significantly impact on the DNA binding parameters of T7 gp2.5. Moreover, we uncover a unique template-catalyzed recycling behaviour of T7 gp2.5, resulting in an apparent cooperative binding to ssDNA, facilitating efficient spatial redistribution of T7 gp2.5 during the synthesis of successive Okazaki fragments. Overall, our findings reveal an efficient binding mechanism that prevents the formation of secondary structures by enabling T7 gp2.5 to rapidly rebind to nearby exposed ssDNA regions, during lagging strand DNA synthesis.

GRAPHICAL ABSTRACT

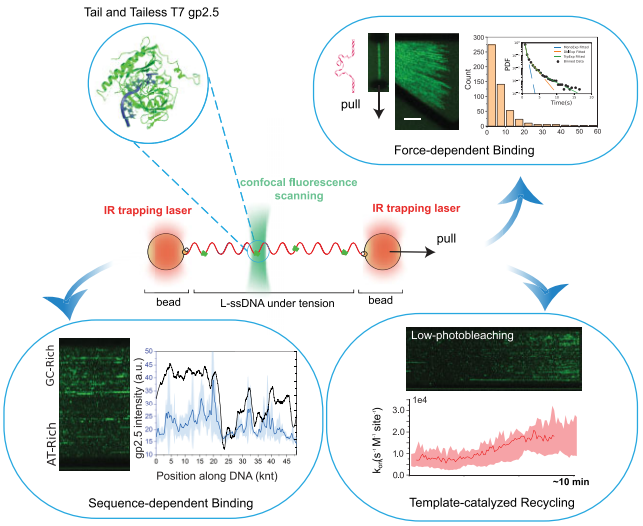

INTRODUCTION

Central to many genome-maintenance machineries are single-stranded DNA binding proteins (SSBs), ubiquitous molecules that have exceptionally high affinity for ssDNA (1,2). A large class of SSBs are known to interact and coordinate with various proteins crucial for DNA replication, recombination, and repair (3–6). Structurally, most SSBs consist of an oligonucleotide binding fold (OB-fold) and a C-terminal tail (7). Ensemble biochemical studies have demonstrated that the OB-binding domain from SSB binds with high affinity to ssDNA, and the C-terminal tail of SSB plays a crucial role in regulating the other protein partner activity (1,7,8). Solution conditions such as the salt composition and concentration (9,10), protein density (11,12),

*To whom correspondence may be addressed. Tel: +31 20 5987987; Fax: +31 20 5987991; Email: g.j.l.wuite@vu.nl
†The authors wish it to be known that, in their opinion, the first three authors should be regarded as Joint First Authors.

as well as template tension (13) have been shown to affect the binding mode or affinity of SSB. Furthermore, the co-replicational binding, i.e. during the gradual generation of ssDNA during replication, has been shown to select the binding mode of SSB to ssDNA (14). In the cell, after binding and acting on ssDNA, the SSB–ssDNA complexes must be bypassed (15), dislodged (15–17) or reorganised (18) along the template to complete DNA metabolism. Thus, the binding dynamics of SSB to ssDNA must be tightly regulated not only to prevent indiscriminate binding and roadblocks but also to define the context-dependent role of the SSB.

Among the SSBs, T7 gp2.5, the SSB protein from the T7 bacteriophage replisome, has a relatively small molecular size (∼25 kDa) and has a monomer binding mode to ssDNA (7). Yet, it features many structural and mechanistic-pathway similarities with higher organisms and thus, it represents an ideal model protein to elucidate the molecular regulation mechanism. T7 gp2.5 has demonstrated that the OB-fold domain is the binding site to ssDNA, thereby protecting bound DNA from degradation by nucleases. Another structural moiety, the T7 gp2.5 acidic C-terminal tail (19–21), has been reported to physically interact with other replication proteins and with the primer-template, contributing to the coordination of leading and lagging strand synthesis at the replication fork (22–28). T7 gp2.5 C-terminal tails are also shown to be essential for DNA recognition and binding (29,30), which competitively exclude the ssDNA from re-annealing (31). Previous studies demonstrate that T7 gp2.5 is a stable homodimer in solution, stabilised by interactions between the acidic C-terminal tails (21,32–35). Yet, it is believed that T7 gp2.5 binds to ssDNA as a monomer, requiring dimers to disrupt prior to binding (21,33). Moreover, several studies using the dsDNA destabilising method and ensemble measurements have reported that T7 gp2.5 has a preferential affinity for ssDNA ranging from $\sim 10^5$ to 10^6 M^{-1} (26,32,34,36,37).

In the context of replication, SSBs are reported to interact with other DNA replicative proteins, e.g. helicase and polymerase (1,2). In addition, considering the fast pace of DNA replication, the SSBs are accordingly required to rapidly coat and redistribute among the exposed single-stranded DNA (ssDNA) of consecutive Okazaki fragments. *Escherichia coli* SSB protein has been recently observed to be recycled between successive Okazaki fragments during lagging strand synthesis (19), which suggests the efficient use of SSB during DNA replication. In the case of T7 replication machinery, the binding and unbinding of T7 gp2.5 must be efficient to achieve the high replication rate and fidelity. Recent studies have revealed the effect of DNA replication on SSB binding to and release from ssDNA (14, 17), emphasizing the importance of understanding the molecular mechanisms underlying these processes. Nonetheless, a mechanistic understanding of T7 gp2.5 binding dynamics originating from the OB domain and acidic C-terminal tail is still lacking; how these binding dynamics are regulated by ssDNA conformation and the base sequence from DNA molecule remains unclear. Furthermore, how the T7 replisome efficiently uses gp2.5 spatially and temporally while maintaining the full function of DNA metabolism is still unclear.

To better understand the molecular regulation of T7 gp2.5 binding dynamics, we have set out to directly observe the binding of fluorescently labelled T7 gp2.5 and a deletion mutant lacking 21 C-terminal residues (gp2.5-Δ21C) to ssDNA using correlated tweezers fluorescence microscopy. Physiological-relevant tension was applied to the ssDNA template to mimic ssDNA conformation. The bound T7 gp2.5 is demonstrated to reduce the contour length of ssDNA by stacking 3 nucleotides in a force-dependent manner with higher binding stability in GC-rich regions. Moreover, the T7 gp2.5 binding suppresses the formation of a secondary structure. The apparent difference in binding dynamics between T7 gp2.5 and gp2.5-Δ21C indicates the regulatory role of the C-terminal tail. We further reveal a unique template-catalyzed recycling behaviour of T7 gp2.5 that results in an apparent cooperative binding to ssDNA. This recycling suggests that the rebinding of T7 gp2.5 might be accelerated due to the presence of a higher local monomer concentration close to the template, which could, in turn, lead to an efficient spatial redistribution of T7 gp2.5 during the synthesis of successive Okazaki fragments.

MATERIALS AND METHODS

Sample preparation

The dsDNA substrates were labeled with terminal biotins allowing for tension-induced melting to generate ssDNA, as described previously by Candelli *et al.* (38). Wild type T7 gp2.5 and gp2.5-Δ21C were purified with a procedure based on previous literatures (10). Purified T7 gp2.5 was labeled with an excess Alexa Fluor® 555 carboxylic acid succinimidyl ester (Thermo Fisher Scientific, Waltham, Massachusetts, USA), following protocols adapted from Etson *et al.* (39) and Kim *et al.* (32). Purified gp2.5-Δ21C without C-terminal tail was fluorescently labelled with Atto647N-maleimide (ATTO-TEC GmbH) following manufacturer's protocol. Detailed procedures on sample preparation can be found in the Supplementary materials.

Single-molecule instrumentation and experiments

The custom-built experimental setup combines dual optical trapping, confocal microscopy, and microfluidics for single-molecule assays. An inverted microscope with a water-immersion objective and a condenser top lens is employed. Two orthogonally polarized, independently steerable optical traps capture streptavidin-coated beads, and their displacement is measured using back-focal plane interferometry. Confocal fluorescence microscopy is performed using a single pulsed laser system for excitation, a fast tip/tilt piezo mirror for scanning, and fiber-coupled avalanche photodiodes for photon counting. A 5-channel laminar flow cell, assembled on an automated XY-stage, allows efficient transfer of optically trapped beads through channels containing molecules of interest. Custom-written software packages using Labview control the optical trapping, microfluidics hardware, and confocal fluorescence, DNA pulling and retracting cycles, and other experimental procedures. Data analysis is conducted using Python, Origin, and MATLAB.

The single-molecule experiments are performed at room temperature in a 5-channel microfluidic flow cell. Laminar flow separates channels for capturing λ-DNA tethers between optically trapped beads, inducing DNA melting, and introducing proteins. Force-distance curves or confocal fluorescence images are recorded individually or concurrently to study the cooperativity and tension effect of SSB on ssDNA binding dynamics.

Data analysis

In this study, we performed a comprehensive analysis of the data collected from single-molecule experiments. The quantification and statistical analysis methods are documented in the following subsections, as well as detailed in the supplementary materials available at NAR online.

Quantification of T7 gp2.5 fractional coverage on DNA and T7 gp2.5 footprint. Confocal fluorescence images of ssDNA were recorded to calculate the fractional coverage of T7 gp2.5 on DNA and its footprint. The average fluorescence intensity signal of bound T7 gp2.5 was determined, and the background intensity was subtracted. The analysis was performed on at least three molecules for each concentration. The footprint of T7 gp2.5 was determined by considering the integrated intensity within the ROI and normalizing by the number of nucleotides in the ssDNA construct. The reported footprint value is the average of 4 DNA molecules incubated with 100 nM of Alexa555-gp2.5.

Mapping the rebinding events of T7 gp2.5. To further quantitively assess the rebinding events of T7 gp2.5, we investigated those fluorescence traces that fall in the rebinding category. The analyzed rebinding traces should meet the criteria: i) two consecutive T7 gp2.5 traces cannot overlap in time and two nearby traces cannot overlap in position, ii) the initial fluorescence intensity of a rebinding event has to be equal or smaller than the final fluorescence intensity of its previous trace, iii) the inter-trace binding time is significantly smaller than the measured k_{on} under our experimental conditions, iv) only those events concatenated in time will be considered. The analysis showed that about 13% of the T7 gp2.5 binding events ($N = 493$) collected under a low-bleaching regime correspond to rebinding events, while only 4% of the binding events ($N = 605$) could be associated with rebinding events under a high-bleaching condition.

Tracking the fluorescent proteins in 1D kymograph. The acquired kymographs were analysed with a custom-written tracking program (40) (MATLAB). Briefly, the position of a fluorescently labelled protein was obtained from a two-dimensional Gaussian fit to the intensity profile in each frame (41,42). The obtained positions were connected to form a trajectory from which the displacement for the different time intervals was determined.

Bleaching correction of the interaction time:. The observed duration of individual fluorescently labelled T7 gp2.5 binding events to ssDNA is shorter than the true interaction time due to photobleaching occurring in our fluorescent experiments. To correct our data for this effect, we followed a protocol adapted from Biebricher et al. (43). The corrected interaction time was then used in subsequent calculations.

Calculation of k_{on} and k_{off} values. A novel technique was proposed for normalizing k_{on} (M^{-1} s^{-1} $Site^{-1}$) to a single binding site by examining the on-rate at a single site and extrapolating to all binding events. The relationship between the average binding time and window size was modeled as a power law, and the single site binding time was calculated. Errors were propagated into k_{on} using the relationship between the single site binding time and its error. The off-rate (k_{off}) was calculated by measuring the binding duration of single trajectories and fitting the distribution with a triple exponential function.

Quantification and statistical analysis. The number of molecules or events analyzed is indicated in the text or figure legends. Errors reported in this study represent the approximated standard error of the mean or was determined by propagating the errors from the fitting coefficients, as indicated in the text.

RESULTS

Single-molecule filming of T7 gp2.5 binding to ssDNA

T7 gp2.5 is a multifunctional protein with an oligonucleotide binding fold (OB-fold) and a flexible C-terminal tail (7), which serve as the ssDNA binding pocket and facilitate interactions with other protein partners during DNA metabolism, respectively. Since no structure of T7 gp2.5 in complex with ssDNA is currently available, we aligned the known structure of T7 gp2.5 with that of the Enc34 SSB, which has been solved in complex with ssDNA (PDB ID: 5odl). The predicted crystal structure of T7 gp2.5 (PDB ID: 1je5) in complex with ssDNA is shown in Figure 1A. This structural alignment suggests that the bases of ssDNA (purple) are stabilized by a mixture of nonpolar residues within the DNA binding cleft of T7 gp2.5. This provides insight into the possible mechanism of T7 gp2.5 binding to ssDNA, which we further investigate using single-molecule visualization techniques.

To investigate the binding dynamics of T7 gp2.5 to DNA at the single-molecule level, we used a combination of high-resolution optical tweezers and confocal fluorescence microscopy (Figure 1B and C), together with a customized microfluidic flow cell. We first visualized the binding of T7 gp2.5 to an ssDNA substrate. To this end, an ssDNA molecule was generated by force-induced melting of lambda-phage (λ) dsDNA (48502 bp) (38) and then incubated in a solution of T7 gp2.5 fluorescently labelled with Alexa555 (see Materials and Methods and Supplementary Materials). Successful binding of multiple T7 gp2.5-Alexa555 proteins to the tethered ssDNA was verified by fluorescence microscopy. A typical confocal snapshot (left panel in Figure 1D) shows individual fluorescent T7 gp2.5 bound to ssDNA. Continuously scanned images along ssDNA axes over time generated a video tracking the dynamic binding picture of fluorescent T7 gp2.5 to ssDNA at the single-molecule level. The 2D kymograph is shown here for simplicity (right panel in Figure 1D). Trajectories of individual fluorescent proteins from the kymograph

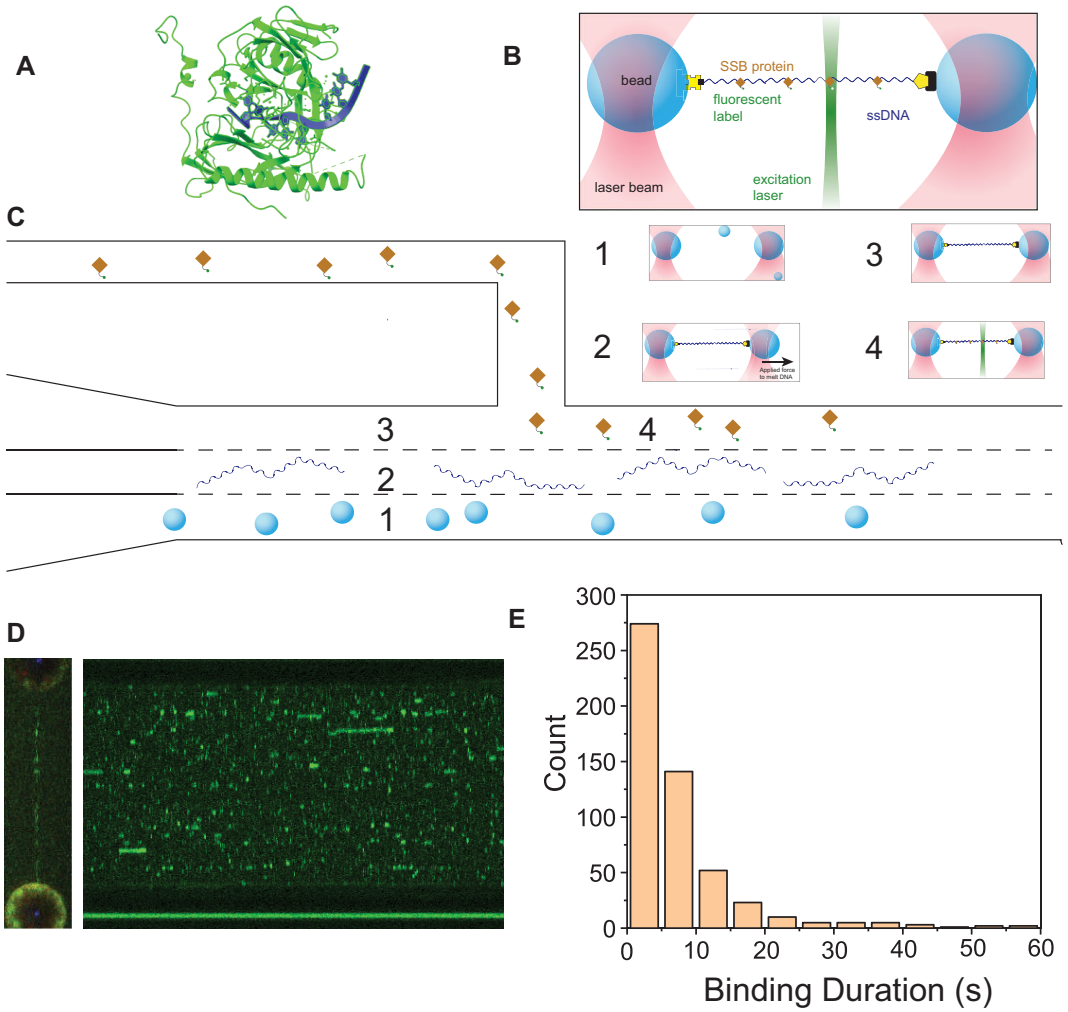

Figure 1. Single-molecule observation of T7 gp2.5 binding on ssDNA. (**A**) The predicted structure of T7 gp2.5 (PDB ID: 1je5) in complex with ssDNA is shown in (A). Since no structure of T7 gp2.5 in complex with ssDNA exists, we aligned the T7 gp2.5 structure to the homologous Enc34 SSB(25), which has been solved in complex with ssDNA (PDB ID: 5odl). The C-terminal tail was not included in the structure. (**B**) Depiction of the experimental setup of a combination of high-resolution optical tweezers and confocal fluorescence microscopy. T7 gp2.5 (orange with red tails) coated biotinylated ssDNA (black) is held between two streptavidin-coated beads (blue) by trapping beams (red), where their position can be manipulated by stretching the DNA. A confocal scanning laser (green) moves back and forth over the ssDNA, exciting the fluorophores (Alexa555) attached to the T7 gp2.5 molecules, creating a fluorescent signal. (**C**) Depiction of the multichannel laminar flow cell. Two beads are optically trapped (1); a single molecule of dsDNA is tethered between the beads (2); the DNA molecule is transported to a channel containing a low-salt content buffer (10 mM Tris–HCl, ph 7.5) where melting is induced by tension; solid black arrow indicates the exerted force by optical trapping (3); the originated ssDNA molecule is then moved to a channel containing gp2.5, where either force-distance curves or confocal fluorescence images are recorded individually or concurrently (4). (**D**) A typical confocal scan (left panel) and kymograph (right panel) show fluorescent T7 gp2.5 bound on ssDNA generated as described in (B). DNA bound with gp2.5 were incubated in solution containing 1, 10, 20, 50, 100 and 500 nM gp2.5-Alexa555 under force of at 3, 6, 12 and 18 pN. As an example, DNA held under 6pN was shown here. Horizontal scale bar: 50s; Vertical scale bar: 2μm. (**E**) Individual trajectory of fluorescent gp2.5-Alexa555 was extracted with a home-written MATLAB program (See Methods). Trajectory data with time v.s. position coordinates were further used to calculate binding duration. As an example, DNA held under 6 pN with 100 nM gp2.5-Alexa555 was shown here ($N = 528$).

were extracted and analyzed with a home-written MATLAB program (see Materials and Methods and Supplementary). Trajectory data with time and position coordinates were then used to calculate the binding duration of the protein, from which the dissociation rate k_{off} can be extracted (see Materials and Method). Figure 1E shows the distribution of binding duration at 6 pN. Moreover, time vs. position coordinates were used to calculate the diffusion constant using the mean-squared displacement (MSD) method. At 12 pN, the apparent diffusion constant of T7 gp2.5 is $(3.9 \pm 3.5) \times 10^{-4}$ $\mu m^2/s$ (Figure S2A). Thus, the bound T7 gp2.5 is measured relatively immobile on ssDNA but not entirely fixed under the examined condition.

Mechanical effect of T7 gp2.5 binding to ssDNA

Based on structural similarities among single-stranded DNA-binding proteins of different species, T7 gp2.5 was proposed to bind to ssDNA by stacking nucleotides between aromatic residues at the OB-fold (21). To determine

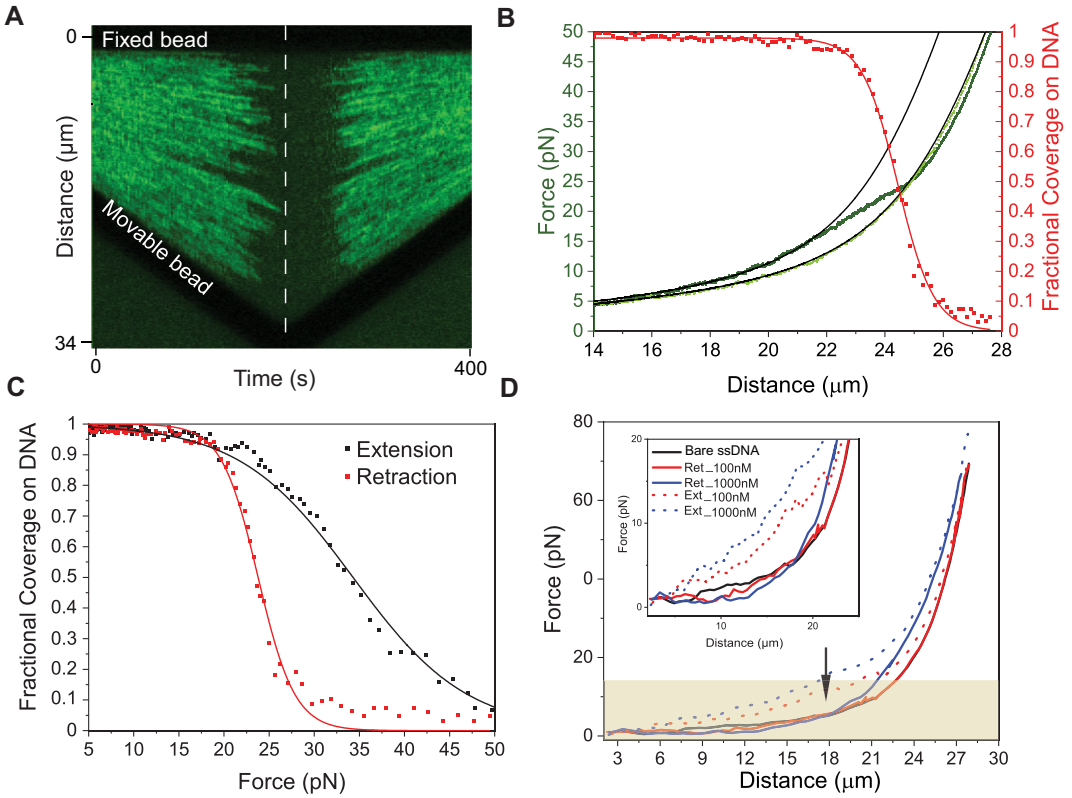

Figure 2. gp2.5 shortens ssDNA by bending it. (**A**) Kymograph corresponding to the extension and retraction bead motions for a ssDNA molecule upon incubation with a solution containing 100 nM gp2.5. The dashed white line indicates the transition between extension and retraction. (**B**) Typical force–distance retraction curves of bare ssDNA (light green, $N = 4$) and ssDNA incubated with 100 nM of gp2.5 (dark green), obtained while recording the kymograph shown in (A). Red dots represent the fractional gp2.5 coverage on ssDNA at each distance during retraction, calculated from the fluorescence data. The solid red line is a guide to the eye. Black solid lines are freely jointed chain fits to both force-retraction curves for the region depicted by the light green rectangle, in which the coverage stays constant and close to saturation. We fitted the extensible freely jointed chain model (eFJC) to both the uncoated and fully T7 gp2.5-coated ssDNA curves (fitting range for bare ssDNA curves: 10 μm and above; fitting range for gp2.5-coated ssDNA curves: 10–22 μm, where ∼95% of gp2.5 still bound on ssDNA, $N = 4$). For bare ssDNA, we obtained a value of contour length $L_c = 25.9 \pm 0.3$ μm (mean ± SEM), while a decreased L_c of 24.4 ± 0.3 μm in the presence of 100 nM T7 gp2.5. (**C**) Fractional gp2.5 coverage on ssDNA at each applied tension during extension (black) and retraction (red) of the molecule. The solid lines are guides to the eye. (**D**) Typical force–distance extension (dotted lines) and retraction (solid lines) curves for ssDNA incubated with gp2.5 at concentrations of 0, 100 and 1000 nM. The red rectangle highlights the tension range where protein binding coexists with the presence of secondary structures on the ssDNA. The black arrow points to the crossing of the retraction curves corresponding to ssDNA incubated with high gp2.5 concentrations and those incubated with low protein concentrations; this crossing is not observed in the extension curves under the same protein concentrations. The *inset* provides a zoomed-in view of the curves within the 0–20 pN tension range for selected graphs. Extension and retraction curves under other gp2.5 concentrations can be found in Figure S2B.

the binding mode and mechanical effect of T7 gp2.5 to ssDNA, continuously scanned kymographs and concurrently obtained force-distance retraction curves were recorded during slow extension and retraction of ssDNA molecules (∼70 nm/s) in a solution containing 100 nM of T7 gp2.5 (Figure 2A and B). Mechanical ssDNA shortening caused by T7 gp2.5 association was observed by comparing curves with and without T7 gp2.5 (Figure 2B). At higher tensions (>∼25pN), both force-distance curves overlap due to few T7 gp2.5 proteins bound on ssDNA. At a tension of around 25 pN and below however, the force-distance curve corresponding to ssDNA in the presence of T7 gp2.5 deviated from the one corresponding to bare ssDNA. In this regime, T7 gp2.5-coated ssDNA showed a shorter end-to-end distance for every given tension.

To determine the shortening and the mechanical effect of gp2.5 binding to ssDNA, we fitted the extensible freely jointed chain model (eFJC) (44) to both the uncoated and fully T7 gp2.5-coated ssDNA curves (the default experimental condition with100nM gp2.5; fitting range for bare ssDNA curves: 10 μm and above; fitting range for gp2.5-coated ssDNA curves: 10 μm to 22 μm, where ∼ 95% of gp2.5 still bound on ssDNA, $N = 4$) (black solid lines in Figure 2B). For bare ssDNA, we obtained values of persistence length $L_p = 1.87 \pm 0.0032$ nm, the stretching modulus $S = 453.11 \pm 9.17$ pN and the contour length $L_c = 25.87 \pm 0.015$ μm (mean ± SEM), in the range of values obtained before (45). In the presence of 100 nM T7 gp2.5, L_p (1.87 ± 0.001 nm) and S (450 ± 10 pN) remained relatively unchanged, while L_c decreased to 24.41 ± 0.012 μm. We have verified that allowing all three parameters (L_p, S and L_c) to vary freely in the fitting process, the best fit is still achieved when L_p and S remain constant while L_c is the only parameter that changes. This supports the conclusion that T7 gp2.5 can shorten ssDNA without significantly altering its rigidity. Furthermore, we chose to fit the

retraction curves rather than the extension curves because the retraction process allows us to start from an 'empty' ssDNA template without potential secondary structure under high tension (∼50 pN) and gradually observe the binding of gp2.5 to ssDNA. In contrast, during the extension process, secondary structures are already present before stretching, which may interfere with the fitting.

We then investigated the shortening contribution per gp2.5 monomer and estimated the footprint of gp2.5 on ssDNA. Having simultaneous access to the fractional coverage using fluorescence microscopy, we related the force-distance retraction curve to the fractional coverage, to assess the contribution of each T7 gp2.5 monomer to shortening. To this end, we first quantified the number of bound T7 gp2.5 monomers in the saturation regime using our intensity per monomer (Figure S1B). In Figure 2B, the contour length shortens approximately 1.46 ± 0.03 μm while 2300 ± 400 monomers are bound, indicating that each T7 gp2.5 shortens ssDNA by 0.6 ± 0.2 nm. The footprint of T7 gp2.5, defined as the space occupied by the protein on DNA and how many bases or base-pairs are protected, was estimated from the integrated intensity in the confocal fluorescence images using ssDNA saturated with T7 gp2.5.

We first estimated the T7 gp2.5 footprint on λ-phage DNA under two hypothetical conditions: without any template tension, where secondary structures are expected to form, and with moderate tension, where we assumed that all secondary structures are resolved. Simulations using UNAFold software (46), indicate that for λ-phage DNA at 24°C, up to 30.5 knt are folded into secondary structures, making only 17.9 knt accessible for T7 gp2.5 binding. Upon background subtraction and using both the fluorescence intensity of a single T7 gp2.5 monomer (Figure S1A), and the available number of nucleotides of our DNA construct (17.9 knt), we obtained a value of 8 ± 1 nt (mean ± s.e.m., $N = 4$ fully coated DNA molecules). In the case that λ-phage ssDNA was fully stretched (48.5 kb) under moderate tension, the space occupied by T7 gp2.5 is one monomer every 22 ± 4nt. It is important to note that these conditions were not meant to suggest that gp2.5 has two distinct binding modes (i.e. two different footprints), but rather to estimate the higher and lower range of the footprint. Systematic errors in our estimation, such as the accuracy of secondary structure percentages under various tensions may have led to an underestimation of the lower bound and an overestimation of the higher bound, resulting in values that might be closer to each other. We then compare the estimated footprint values with the intrinsic site-size of gp2.5. For gp2.5, the intrinsic-site size as measured by intrinsic fluorescence quenching (8) is 7–8 nts of ssDNA, matching with the lower limit of the footprint determination (i.e. 8 nt). This agrees very well with the crystal structure of the spherical diameter of gp2.5 and its closely related Enterobacter phage Enc34 SSB which shows 7–8 nt occluded by the OB-fold (25).

Next, we investigated the force effect on T7 gp2.5 binding to ssDNA by quantifying the coverage at each tension for both the extension and retraction traces (Figure 2C). When extending a T7 gp2.5-coated ssDNA molecule, only tensions above 25 pN resulted in a progressive reduction of the coverage and, at a tension of about 50 pN, most of the T7 gp2.5 is forced off the ssDNA molecule. In contrast, when relaxing the molecule from a tension of ∼50 pN with a same rate, we did not observe T7 gp2.5 binding until the tension dropped below 30 pN. In this case, we could only restore full coverage at a tension of 20 pN and below. This non-equilibrium hysteretic binding behaviour suggests that T7 gp2.5 association is more sensitive to force compared with T7 gp2.5 dissociation. T7 gp2.5 shortens the ssDNA upon binding; such shortening by DNA bending must act against the applied force, thereby resulting in the high sensitivity to force we observed. Nevertheless, once bound, the protein is rather stable on the ssDNA i.e. it is able to resist higher forces.

To investigate the interaction between T7 gp2.5 and ssDNA in the presence of coexisting secondary structures, we first collected retraction force-distance curves at a speed of ∼70 nm/s and a starting tension that exceeds the presence of secondary structures (47). Subsequently, we introduced the ssDNA template to a solution containing 100 nM of T7 gp2.5. Our observations revealed that ssDNA coated with T7 gp2.5 displayed a longer end-to-end distance at low force regimes (<∼15 pN, see Figure 2D) in comparison to bare ssDNA. This finding suggests that T7 gp2.5 may bind to ssDNA prior to potential secondary structure formation, effectively suppressing secondary structures, such as hairpins (red area in Figure 2D and inset). It is crucial to highlight that the contour length elongation was only significant at higher protein concentrations, as demonstrated by the retraction curves at higher concentrations intersecting those at low protein concentrations (black arrow, inset Figure 2D).

Conversely, extension force-distance curves, which were obtained by starting at low force (∼0 pN, where secondary structures form before protein binding) and increasing the force to ∼50pN (∼70 nm/s), did not exhibit contour length elongation at low force regimes. Moreover, there was no crossover between high-concentration and low-concentration curves (Figure 2D, inset). This observation indicates that pre-formed secondary structures may not be resolved by gp2.5 binding.

Binding and unbinding dynamics of T7 gp2.5 and gp2.5-Δ21C

The flexible C-terminal domain of T7 gp2.5 has been reported to interact and coordinate with other DNA-associated proteins, e.g. DNA polymerase and DNA helicase within a replisome (19–21). Previous studies also suggested that C-terminal tail of T7 gp2.5 plays a crucial role in stabilizing a homodimer of T7 gp2.5 in the solution which later dissociates into monomer upon binding to ssDNA (32–34,37,47). Thus, the C-terminal tail is believed to play a critical role in regulating the binding and unbinding dynamics of T7 gp2.5. We investigated the effect of C-terminal tail on association (on-rate) and dissociation (off-rate) of T7 gp2.5 and gp2.5-Δ21C under various template tensions (3, 6, 12 and 18 pN) (Figure 3A).

In this single-molecule study, we examined the on-rate at a single binding site for a given concentration (k_{on}, $M^{-1}\ s^{-1}\ site^{-1}$) at applied tensions of 3, 6, 12 and 18 pN for both T7 gp2.5 and gp2.5-Δ21C. The time interval between the start point of one binding event and the next subsequent

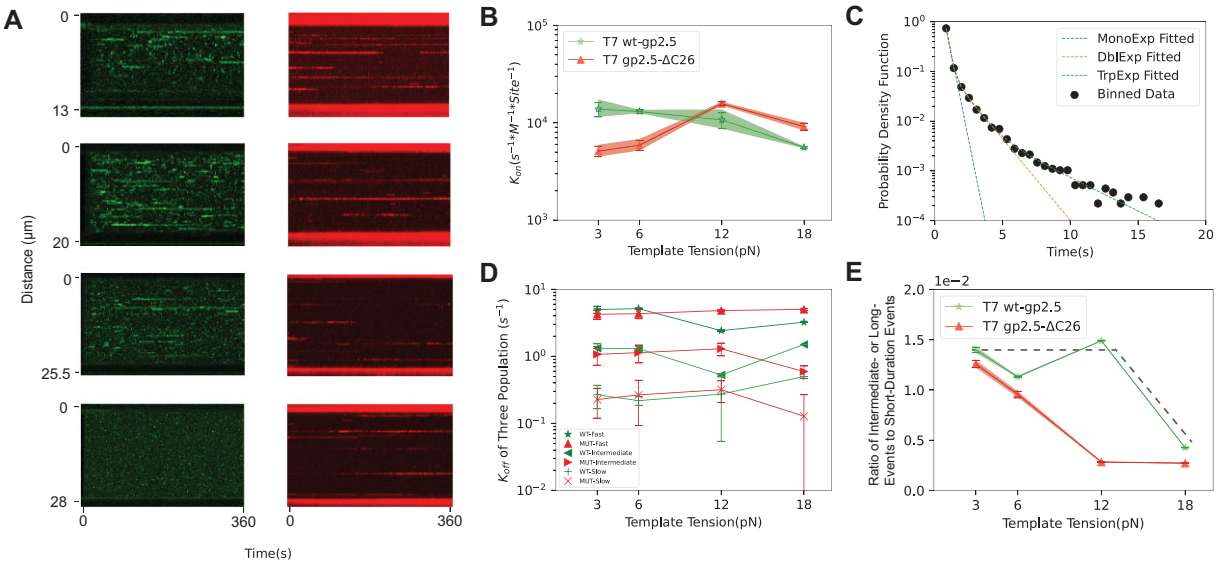

Figure 3. Probing the effect of C-terminal tail of gp2.5 on binding and unbinding dynamics under various template tension. (**A**) Kymographs resulting from incubating ssDNA in a buffer containing 20 nM fluorescently labelled T7 wild-type gp2.5 or 42.5 nM T7 gp2.5-ΔC21 under 3, 6, 12 and 18 pN. The trajectories are extracted as described in Method section. (**B**) Comparison of on-rates k_{on} between T7 gp2.5 (green star) and gp2.5-ΔC21 (red triangle) under various template tensions. (**C**) Triple exponential fit of T7gp2.5 binding durations shown as an example at 6 pN. Binding durations can be captured mostly with a triple exponential distribution, with durations falling into three categories, short-, intermediate- and long-lived, corresponding to the regimes of the monoexponential fit (blue), the double exponential fit (red) and the triple exponential fit (green). The short interactions correspond to non-specific binding, whereas the intermediate and long interactions are specific binding. (**D**) Comparison of the off rates (k_{off}) on ssDNA template between T7 gp2.5 and gp2.5-ΔC21 observed at various template tensions and for different populations (see legend). (**E**) Comparison of the ratio on specific (intermediate and long) events to non-specific (short) events for T7 gp2.5 and gp2.5-ΔC21 observed at various template tensions. Dotted lines are a guide to the eyes to show the general trend for T7 gp2.5.

binding event was analyzed by varying the spatial windows of the kymograph, allowing the capture of a single site's kymograph width through fitting (see Materials and Methods, Supplementary Materials, and Figure S3). Initially at low tension (3–6 pN), T7 gp2.5 protein with a C-terminal tail shows a higher on-rate k_{on} ($14 \pm 3 \times 10^3$ M^{-1} s^{-1} $site^{-1}$) than that of the mutant gp2.5-Δ21C protein ($5.1 \pm 0.7 \times 10^3$ M^{-1} s^{-1} $site^{-1}$), possibly benefiting from the C-terminal tail assisting in binding with secondary structures. As tension. increased (6–12 pN), the on-rate k_{on} of the wt T7 gp2.5 protein decreased with tension, while for gp2.5-Δ21C, k_{on} increases with tension up to 12 pN and subsequently declined (Figure 3B). The observed increase in binding of T7 gp2.5-ΔC21 within a given observation time window, as evidenced by a higher on-rate, may be attributed to the availability of more ssDNA binding sites due to tension disrupting secondary structures, which exist at tensions below ∼15 pN (47). At even higher tension on ssDNA after all the hairpins are fully opened (18pN), the binding of mutant T7 gp2.5-ΔC21 also decreased, as anticipated. Supplementary Table 1 and Figure S4 provide a summary of k_{on} values. The monotonic decrease of T7 gp2.5 is consistent with the aforementioned observations, demonstrating the force-dependent binding of T7 gp2.5. In comparison, the wild-typed T7 gp2.5 exhibited a lower final k_{on} value ($5.59 \pm 0.04 \times 10^3$ M^{-1} s^{-1} $site^{-1}$) than the truncated T7 gp2.5-ΔC21 ($9.1 \pm 0.8 \times 10^3$ M^{-1} s^{-1} $site^{-1}$) at 18pN. This difference may be due to the wild-type protein's negatively charged C-terminal tail, which further reduces binding due to repulsion from the negatively charged ssDNA backbone.

Next, we assessed how the C-terminal tail of T7 gp2.5 impacts the unbinding rate (k_{off}) under various template tensions. We measured the binding duration of each fluorescently labelled protein from the kymograph (Figure 3A) and plotted the distribution of binding durations for all binding events. After correcting for fluorophore photobleaching occurring in our experiments, following the methodology reported previously (43) (see Materials and Methods and Figure S1 in the Supporting Material), we obtained an average k_{off} (1/average-binding-duration) value of 6.3(±0.2) s^{-1} for wild-type T7 gp2.5, and k_{off} value of 5.2(±0.6) s^{-1} for gp2.5-Δ21C at 6 pN of template tension. The measured longer average life duration ($1/k_{off}$) of gp2.5-Δ21C on ssDNA indicates that deleting C-terminal tail increases the stability of T7 gp2.5–ssDNA complex. The flexible negative-charged C-terminal tail from wt T7 gp2.5 competes with the OB domain for this interaction and might enhance the rate of dissociation of T7 gp2.5.

To parse the unbinding rate and capture most of the unbinding characteristics, the distribution was fitted with a triple exponential function (Figure 3C), and the total binding duration was divided into three components corresponding to the terms of the triple exponential fit:

$$y = A_1 e^{-k_1 t} + A_2 e^{-k_2 t} + A_3 e^{-k_3 t},$$

where A_1, A_2 and A_3 correspond to the relative weightings of the different population proportions, and k_1, k_2 and k_3 correspond to the unbinding rates of the short, intermediate, and long-lived populations. For wt gp2.5 at 6 pN, the rate constants k_1, k_2 and k_3 are 5.1 ± 0.1, 1.3 ± 0.1 and

0.22 ± 0.03 s^{-1} respectively. For gp2.5-ΔC26 at 6 pN, k_1, k_2 and k_3 are 4.3 ± 0.6, 1.1 ± 0.3 and 0.3 ± 0.2 s^{-1} respectively. Supplementary Table 1 and Figure S5 provide a summary of k_{off} values. These rate constants do not show significant force dependence (Figure 3D), but the state proportions do shift as a function of force, where higher forces decrease the proportion of long-lived (specific) events for both wild-typed and mutant protein (Figure 3E).

We found that an increasing tension on the ssDNA (from 3 to 18 pN) resulted in a stable unbinding rate (k_{off}), within the fast, intermediate and long-lived populations for both wild-type T7 gp2.5 and mutant gp2.5-Δ21C (Figure 3D); however, the proportion of events that belong to intermediate or long-lived states decreases with tension (Figure 3E). This finding supports the model that T7 gp2.5 induces compaction of ssDNA upon binding, which is opposed by DNA tension. The force dependence of the intermediate- and long-lived state proportions suggests that these both depend on DNA tension, and there may be two sequential DNA bending steps. Roughly 1% of binding events last for intermediate timescales or longer, and ∼0.05% of binding events last until long duration. The stoichiometric influence of the different populations must consider their different rates, in terms of coverage, using the same force level of 6 pN, for T7 gp2.5, 96 ± 10% of coverage is provided by the short-lived events, 4 ± 1% by intermediate events, and 0.7 ± 0.3% by long events. For gp2.5-Δ21C at 6pN the coverage is 96 ± 16% short events, 4 ± 2% intermediate events and 1 ± 1% long events (Table S1).

Sequence-dependent binding of T7 gp2.5

The interaction of proteins with DNA can be influenced by the sequence-dependent properties of DNA, such as the formation of secondary structures and their stability. T4 gp32 and *E. coli* SSB proteins are reported to act through the inhibition of refolding (48). Therefore, sequence-dependent effects on binding dynamics are conceivable, given the distinct folding timescales for GC-rich and AT-rich hairpins (49). Despite this, bulk biochemical results have suggested that SSB binding is sequence independent. In this study, we aimed to investigate the impact of DNA sequence on T7 gp2.5 binding dynamics at the single-molecule level with significantly improved spatial and temporal resolution. To achieve this, we utilized a ssDNA construct derived from λ-phage DNA, where half of the sequence is relatively AT-rich, and the other half is relatively GC-rich. Kymographs were obtained by incubating ssDNA in a buffer containing ∼20 nM of T7 gp2.5-Alexa555 at 12 pN (Figure 4A).

Following the previously established analysis methodology (50), we determined the orientation of ssDNA and observed that more T7 gp2.5 was bound at the GC-rich region rather than at the AT-rich region of the ssDNA from the kymograph (Figure S6). To quantitatively show the effect of base sequence on T7 gp2.5 binding, the averaged fluorescence intensity resulting from fluorescent T7 gp2.5 bound on ssDNA was plotted as a function of the GC-content of λ-DNA. The fluorescence intensity from kymographs taken under the same conditions as the one in (Figure 4A, Figure S6) were averaged ($N = 4$) after individually orienting them to the best (anti)correlation with the GC-content plot. The GC-content of λ-DNA was calculated in 200-nt window bins and plotted in solid black, blue (Figure 4B). The correlations for the different conditions are plotted in Figure 4C, showing a stable correlation between T7 gp2.5 fluorescence intensity and GC content at forces under 18 pN; as a comparison, the mutant gp2.5-Δ21C show little or no correlation for at forces 6pN and over.

The difference in binding affinity between AT and GC-rich regions can be determined by pooling the events from either region. We observe differences in the duration distribution between the AT-rich and GC-rich regions: particularly the number of events with an intermediate-time scale duration appeared larger in the GC-rich region (Figure 4D). One caveat, this shift occurs in the proportions of intermediate and long-lived states, so the proportion of events that last to intermediate or greater timescales is higher for GC-rich DNA as opposed to AT-rich DNA. This finding is also reflected in the relative intermediate population ratio, a measure of the relative abundance of the states, is greater for GC-rich regions, and far more tightly clustered (Figure 4E). The influence of k_{on} and k_{off} on GC-content were also analyzed and shows a high correlation coefficient $R^2 = 0.69$ for k_{off} in GC-rich regions.

T7 gp2.5 displays template-catalyzed recycling and cooperatively binding

We monitored T7 gp2.5 binding to ssDNA over an extended period (>500 s) under high photobleaching (inter-scan interval of 6 ms, Figure 5A, top panel) and low photobleaching (inter-scan interval of 1000 ms, Figure 5A, bottom panel) conditions. The frequency of binding events increased under low photobleaching conditions (Figure 5A, bottom panel) and was not observed with tailless mutant gp2.5-Δ21C (Figure 5B). This increased binding rate, unreported in previous short-term studies or high bleaching conditions, was observed over a relatively long-time range (>8 min). Analyzing the on-rate and off-rate using methods from Figure 3B and C revealed an increased on-rate (Figure 5C, top panel), suggesting T7 gp2.5 efficiently rebinds to neighboring sites and supports a template-catalyzed recycling model (Figure 5D). Interestingly, a decreased off-rate was also observed (Figure 5C, bottom panel), indicating longer-lasting T7 gp2.5 binding as more protein accumulates, potentially due to longer-lived proteins displacing shorter-lived binding events.

We assessed T7 gp2.5 coverage on ssDNA as a function of fluorescently labeled Alexa555-gp2.5 concentration using confocal fluorescence microscopy. Protein binding to ssDNA increased with concentration, saturating at ∼50 nM (Figure 5E), while binding to dsDNA remained negligible even at the highest concentration (Figure 5E). This confirms T7 gp2.5's preferential binding to ssDNA over dsDNA (4,51).

We fitted the concentration-dependent coverage using the McGhee-von Hippel model (52,53) (Figure 5F), which characterizes protein-DNA binding with three parameters: (i) equilibrium binding constant K_d (M-1), (ii) cooperativity factor ω, and iii) protein footprint n (number of nucleotides). Fitting the data with two previously obtained footprint values (8 nt and 22 nt) and assuming secondary

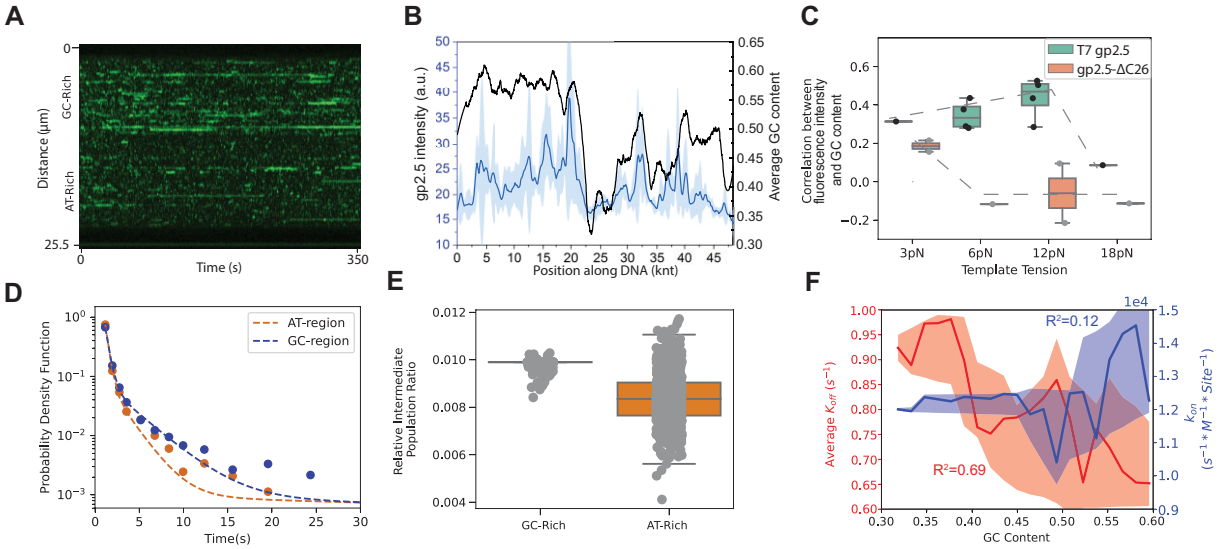

Figure 4. Sequence-dependent binding of T7 gp2.5. (**A**) Kymograph resulting from incubating ssDNA in a buffer containing ∼20 nM of gp2.5-Alexa555 at 12 pN. (**B**) AT-content of λ-DNA (solid black, green, in 200-nt bins) and, in blue, averaged fluorescence intensity from kymographs taken under the same conditions as the one in (A), which were previously individually oriented to the best (anti)correlation with the AT-content plot ($N = 4$). The fainted blue area represents the SD of the gp2.5-Alexa555 averaged intensity. (**C**) Boxplot for correlation between intensity and GC content for T7 gp2.5 and gp2.5-ΔC21 under various template tensions. Bands are the first and third quartiles, with the mean as the center line. Dotted lines are a guide to the eyes to show trends for T7 gp2.5 (flat or rising until 12 pN, dropping at 18 pN) and gp2.5-ΔC21 (Dropping to approximately zero correlation at 6 pN and over). (**D**) Probability distribution plot of the duration of binding events observed at the GC region (red, $N = 266$) and AT-region (orange, $N = 221$) at 12 pN. Events in each region are fit to a double exponential model (there were insufficient statistics for a triple exponential). A divergence is seen on the intermediate timescale, where fewer binding events last to intermediate timescale in the AT-rich region. (**E**) Comparison of intermediate population ratios, that is the relative proportion of intermediate to total events, for the GC-rich and AT-rich regions. There is a greater proportion and a lower variance in the GC-rich region, possibly owing to sequence dependent effects in binding. (**F**) Plot of k_{off} and k_{on} as a function of GC, content. k_{on} (blue) increases with GC content, whereas k_{off} (red) decreases with increasing GC content.

structure in presence (i.e. 8 nt), we derived a cooperativity factor ω of 110(±40). This suggests T7 gp2.5 is ∼100 times more likely to bind adjacent to a bound monomer than to a random ssDNA site. The non-cooperative model variant did not fit the data (Figure 5F, solid lines).

The McGhee-von Hippel fits yielded binding constants of 1×10^6 M^{-1}, with footprints of 8 nt. These values represent the intrinsic affinity of T7 gp2.5 for ssDNA without considering its cooperativity. Since previous studies reported observed affinity constants, we used the product Kω for comparison, representing both the binding constant and cooperativity factor. Our experiments yielded a Kω value of ∼1.1×10^8 M^{-1}. Considering the maximum accessible binding sites of λ-phage DNA (48 knt/8 nt = 6k sites), the apparent affinity constant will be ∼1.8×10^4 M^{-1} $site^{-1}$ (1.1×10^8 M^{-1}/6k sites), which is very similar to our previously calculated value of $(1.3 \pm 0.056) \times 10^4$ M^{-1} $site^{-1}$ at 6 pN (Supplementary Table 1).

DISCUSSION

In this study, we employed correlated tweezers fluorescence microscopy to directly visualize fluorescently labelled T7 gp2.5 and its tailless mutant gp2.5-Δ21C binding to ssDNA at the single-molecule level. This approach enabled us to investigate the molecular regulation of T7 gp2.5 binding dynamics. Our interpretation of the C-terminal tail, ssDNA conformation, and base sequence regulating T7 gp2.5 binding to ssDNA is summarized in Figure 6, which illustrates the varying binding dynamics of T7 gp2.5 and gp2.5-Δ21C to ssDNA as a function of template tension (Figure 6).

T7 gp2.5 binding to ssDNA exhibits a general monotonic decrease trend with tension (Figure 6, left to right). Under low tension conditions (3–6 pN), where ssDNA is prone to forming secondary structures, the tail of T7 gp2.5 interacts with ssDNA, resulting in an elevated binding affinity (k_{on} value) in comparison to its tailless mutant (Figures 3B and 6A, B). The C-terminal tail may engage with ssDNA secondary structures due to its flexibility and diverse molecular interactions, compensating for electrostatic repulsion between the tail and ssDNA backbone and promoting more effective binding at low tensions. As tension on ssDNA increases (6–12 pN), leading to the suppression of secondary structure formation, T7 gp2.5-ΔC21 exhibits increased binding to ssDNA, attributed to the enhanced availability of binding sites (Figures 3B and 6C). The negative charge of the C-terminal tail presents a barrier to binding with the negatively charged ssDNA backbone, resulting in a diminished k_{on} value relative to T7 gp2.5-ΔC21 (Figure 6D). At high tension (∼18 pN), when all hairpins open, both T7 gp2.5 and mutant T7 gp2.5-ΔC21 exhibit decreased binding affinity. This decrease is likely attributable to the tension impeding the proper arrangement of bases within the gp2.5 binding pocket (Figure 6E, F), as well as the wild-type protein's negatively charged C-terminal tail, which further undermines binding due to repulsion from the negatively charged ssDNA backbone. In addition, we identified three distinct modes of T7 gp2.5 binding to ssDNA:

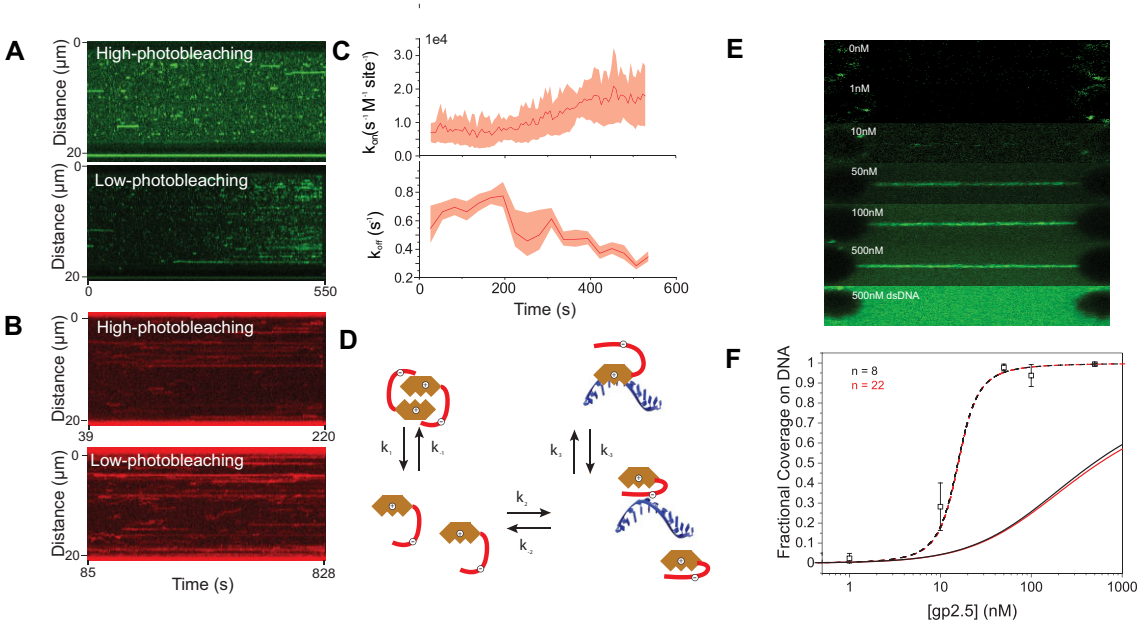

Figure 5. T7 gp2.5 displays template-catalyzed recycling and thus apparent cooperatively binding. (**A**) Kymographs resulting from incubating ssDNA in a buffer containing ∼20 nM of gp2.5-Alexa555 at 12 pN, using inter-scan interval of 6 ms (top panel, high-photobleaching condition) and 1000 ms (bottom panel, low-photobleaching condition). (**B**) Kymographs resulting from incubating ssDNA in a buffer containing ∼100 nM of T7 gp2.5-ΔC21-Atto647N under 12 pN, using inter-scan interval of 6 ms (top panel, high-photobleaching condition) and 1000 ms (bottom panel, low-photobleaching condition). Please be noted high-bleaching condition with Atto647N dye would result in extremely fragile ssDNA due to photoirritation and it is quite challenging to get longer observation. (**C**). k_{on} increases with time as more material accumulate on the ssDNA in the low photobleaching condition for T7 gp2.5-Alexa555, suggesting a cooperative binding mechanism (top panel); while k_{off} decreases with time, meaning that any T7 gp2.5 bound to the ssDNA last longer as time goes on and more material accumulates (bottom panel). This effect can possibly be attributed to longer-lived material surviving and displacing shorter-lived binding events. (**D**) Our proposed template-catalyzed recycling of gp2.5 model. When wild type gp2.5 binds to ssDNA, it needs first to break the dimer, which is a reversible reaction. Once a monomer gp2.5 molecule is bound on ssDNA, it will, after dissociation, be more readily available to directly rebind than the monomers that need to be formed by dimers falling apart. (**E**) Confocal fluorescence images of DNA held at 6 pN, upon incubation with increasing concentrations of fluorescently labeled Alexa555-gp2.5 from 0nM to 500nM. (**F**) gp2.5 fractional coverage on DNA for increasing protein concentrations (mean ± s.d., $N \geq 3$). Dashed lines represent the Mc-Ghee-von-Hippel fit to our data and solid lines represent a fit to the version of the model, which assumes no cooperativity of the binding. The models were fit in both cases by using either a footprint of 8 (black dashed curves) or 22 (red dashed curves) nucleotides.

rapid and unspecific collision (G1 population), intermediate binding (G2 population), and prolonged binding (G3 population) (Figure 6G). Our investigation of sequence-specific binding dynamics revealed that T7 gp2.5 exhibits a preferential binding affinity for GC-rich sequences as opposed to AT-rich sequences (Figure 6H).

Evidence for T7 gp2.5-induced ssDNA bending and inhibition of secondary structure formation

When a significant fraction of the ssDNA template was coated with T7 gp2.5, we observed a reduction in contour length with negligible alterations in persistence length or stretch modulus (Figure 2A, B). A shortening of approximately 0.6 nm per bound protein aligns with the model proposed by Hollis *et al.* (7), which suggests T7 gp2.5 stacks nucleotide bases between the aromatic residues present in the OB-fold. These observations support the hypothesis that T7 gp2.5 shortens ssDNA by bending it. Our direct observation of T7 gp2.5 also reveals relatively low mobility on ssDNA, distinguishing it from other diffusive SSBs, such as *E. coli* SSB (54). This static binding may result from the stacking interaction between base-aromatic residues, which also contributes to the contour length shortening of the DNA template.

T7 gp2.5 serves a crucial role in DNA metabolism by suppressing secondary structures (4). Two competing hypotheses exist concerning the underlying mechanism: either preventing secondary structure formation or resolving existing structures. Our measurements demonstrate that slow retraction curves exhibit longer end-to-end distances than bare ssDNA at low force regimes (<∼15 pN), while slow extension curves do not. This evidence supports a model in which T7 gp2.5 prevents ssDNA from folding into secondary structures rather than disrupting pre-existing ones (Figure 2D and inset). Although a weak interaction between secondary structures and the C-terminal tail is suggested by a higher on-rate than its tailless mutant (Figure 3B), this characteristic implies that T7 gp2.5 must efficiently bind to ssDNA to outcompete hairpin formation.

Regulation of T7 gp2.5 binding dynamics by its C-terminal tail, template conformation and sequence

Our single-molecule visualization of the binding of T7 gp2.5 and its tailless mutant to ssDNA demonstrates a molecular regulation by both the substrate (i.e. template conformation and sequence) and the protein (i.e. the C-terminal tail of gp2.5). The binding constant of T7 SSB protein arise from

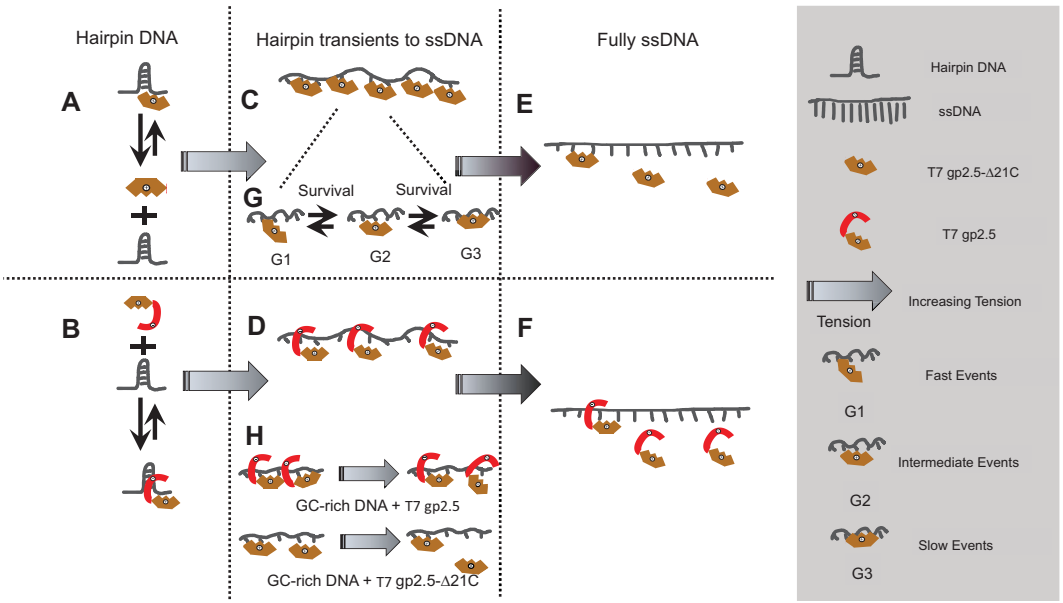

Figure 6. Schematics of T7 gp2.5 binding to ssDNA regulated by C-terminal tail, ssDNA conformation, and base sequence (increasing template tension from left to right). (**A**) and (**B**) show the binding interaction of wild-type T7 gp2.5 and mutant T7 gp2.5-ΔC21 to ssDNA under low tension respectively, where ssDNA mostly forms secondary structure (e.g.: hairpin shown here as an example). The tail of T7 gp2.5 assists the binding to ssDNA as indicated by a higher k_{on} value at 3 pN (Figure 3B). (**C**) shows that ssDNA exposes more available binding sites with an increasing template tension applied on ssDNA, thus more T7 gp2.5-ΔC21 binds to ssDNA. (**D**)The negative charge of the C-terminal tail decreases the binding to the negatively charged ssDNA backbone, thus showing a decreasing k_{on} value compared with truncated T7 gp2.5-ΔC21 (Figure 3B). (**E** and **F**) With more tension on ssDNA the hairpin fully opened and both T7 gp2.5 and mutant T7 gp2.5-ΔC21 have a decreased binding affinity. (**G**) The binding of T7 gp2.5 shows multiple states: by fast and unspecific collision (G1 population), by specific intermediate (G2 population) and by long (G3 population) binding events. (**H**) T7 gp2.5 shows a preferred specific binding to GC-rich sequence over AT-rich sequence.

the interplay between these factors. Interactions between T7 gp2.5 and different ssDNA conformations are studied under various template tensions. Our findings suggest that a significant proportion of secondary structure on the template could reduce gp2.5 binding due to limited binding sites. As secondary structures transition to fully ssDNA, gp2.5 binding affinity increases because of the availability of more binding sites. However, a stretched template with tension applied on the backbone of fully opened ssDNA suppresses gp2.5 binding, as the association requires DNA backbone bending, which is unfavorable under tension.

Wild-type T7 gp2.5 has a lower k_{on} than gp2.5-Δ21C when secondary structures are fully disrupted (∼18 pN). This may be attributed to the C-terminal tail stabilizing dimer formation, as supported by previous studies (10). The local concentration of protein decreases by half upon dimer formation, reducing T7 gp2.5 binding frequency to ssDNA. In contrast, the mutant gp2.5-Δ21C demonstrates a longer average life duration ($1/k_{off}$) than the wild-type protein, suggesting that deletion of the C-terminal tail also functions in regulating the unbinding dynamics of T7 gp2.5.

We propose a kinetic model for dimeric T7 gp2.5 interaction with DNA based on the triple exponential parsing of unbinding dynamics. The model suggests that T7 gp2.5 encounters DNA, dissociates into a monomer, binds to, and bends template through two further proceeding steps. Heterogeneous binding durations may be explained by factors such as the presence of secondary structures and sequence content near the binding site. Our data reveal that T7 gp2.5 exhibits a preference for binding to GC-rich sequences, as indicated by a higher binding affinity (k_{on}) and a lower off-rate (k_{off}) compared to AT-rich sequences (Figure 4). This preferential binding may arise from steric interactions between the amino acids of the gp2.5 binding pocket and the base pairs of the ssDNA.

The differential dynamics observed in the k_{off} rates predominantly occur within intermediate and longer-lived states, suggesting that the sequence-dependent binding dynamics are attributable to the bending process. Furthermore, the local sequences in the template, which have the potential to form secondary structures, may modulate the binding affinity of gp2.5. The distinct binding abilities of gp2.5 to GC-rich and AT-rich sequences primarily stem from the inherent differences in the base pairs and the consequent secondary structures, which subsequently influence the binding dynamics of gp2.5.

In our investigation, we identified three distinct regimes of binding duration for gp2.5: rapid, intermediate, and prolonged. The biological implications of these distinct binding populations remain unclear, but we propose that they may serve specific roles in DNA metabolism. Rapid-binding events may allow for efficient displacement by the translocating DNA polymerase while concurrently suppressing the formation of secondary structures. Intermediate events may function as temporary protection for ssDNA, and long-binding events provide more stable protection for longer exposed ssDNA regions during lagging strand synthesis. By adapting its binding dynamics to the local ssDNA environment, T7 gp2.5 can efficiently protect, stabilize, and manage ssDNA during DNA replication.

Template-catalyzed recycling enables efficient use of T7 gp2.5

Our study reveals that T7 gp2.5 demonstrates increased on-rates (Figure 5C, top panel) and decreased off-rates (Figure 5C, bottom panel) under low photobleaching conditions over an extended period. This increase in on-rate suggests that T7 gp2.5 can efficiently rebind to neighbouring sites on the ssDNA, as opposed to binding to the ssDNA-gp2.5 complex with free proteins from the solution. The decrease in the off-rate indicates that T7 gp2.5 bound to the ssDNA remains bound longer as more protein accumulates over time. These observations led us to consider protein recycling as a possible mechanism instead of the classical cooperative binding. The recycling model posits that once a T7 gp2.5 monomer dissociates from the ssDNA; it can quickly rebind to a nearby site rather than relying on a free-protein from solution to bind to the ssDNA-gp2.5 complex. Additionally, the tailless mutant of T7 gp2.5 binding with higher on-rate values under specific tensions (Figure 3B) further supports the recycling model. The tailless mutant lacks the C-terminal tails, which leads to a reduced energy barrier for dimer disruption, allowing the mutant to bind more quickly to ssDNA. This observation implies that dimer disruption is a rate-limiting step for T7 gp2.5 binding, highlighting the importance of monomer availability in the rebinding process.

The rebinding of T7 gp2.5 could result in apparent cooperativity. T7 gp2.5 is known to bind ssDNA as a monomer, while it exists as a dimer in solution (7,10,55). The dimeric form of T7 gp2.5 exhibits additional stabilization via interactions between two C-terminal tails in trans (51), leading to a higher free energy barrier for tail opening. The tailless mutant's higher on-rates under 12pN and 18pN tension support this notion. We propose that the DNA template acts as a catalyst to produce monomeric T7 gp2.5, explaining the increase in T7 gp2.5 binding.

The observed cooperativity values may be attributed to T7 gp2.5 homodimers dissociating near the ssDNA template, resulting in improved binding affinity in proximity to bound SSB. Cooperativity is common among T7 gp2.5 analogues from other species (56,57), as ssDNA-binding proteins need to interact and rapidly coat exposed ssDNA. Our study shows that T7 gp2.5 has lower cooperativity than analogues from other species, such as T4 gene 32 protein, *E. coli* SSB, or human RPA, consistent with previous findings (34,51,56–58). Although high cooperativity values have been determined before for the T4 bacteriophage gene 32 protein ($\omega \sim 10^3$) (56), or yeast, y-RPA ($\omega \sim 10^4$–10^5) (57), a previous Electron Microscopy study of T7 gp2.5 has reported much lower cooperativity (4). Differences in experimental conditions, such as DNA templates and salt concentrations, could contribute to the observed discrepancies in cooperativity values.

Our results suggest a recycling mechanism for T7 gp2.5, which is highly effective in rapidly binding to newly exposed ssDNA regions during Okazaki fragment synthesis. This mechanism is supported by recent findings on *E. coli* SSB (19), which also demonstrate concentration-dependent internal recycling. The rapid replication of T7 bacteriophage necessitates an efficient binding mechanism for T7 gp2.5 to cope with the fast pace of replication. Recycling allows coverage without needing to upregulate expression levels for SSB protein, i.e. it is the most efficient way to ensure replication fidelity without needing to overexpress the protein. If there is no recycling, then the number of SSBs required would be proportional to the total length of ssDNA at any time during the replication. With 100% recycling the number of copies of SSB required would only need to be enough to coat the longest individual segment of Okazaki fragment DNA. This highlights the relevance of the recycling process, even if its probability of occurrence or detection is low. We hypothesize that T7 gp2.5 recycling might be further optimized through interactions between its C-terminal tail and other replisome proteins or T7 gp2.5 monomers, thereby increasing local concentration and facilitating redistribution near emerging ssDNA during processive replication. Our findings emphasize the fundamental role of T7 gp2.5 in replication, contrary to its previous designation as an 'accessory' protein.

DATA AVAILABILITY

The datasets generated and/or analyzed during the current study, as well as the codes for image trajectory analysis are available from the corresponding author on reasonable request/ and have been archived on Zenodo, https://doi.org/10.5281/zenodo.7896382.

SUPPLEMENTARY DATA

Supplementary Data are available at NAR Online.

ACKNOWLEDGEMENTS

We thank R. Jhingoerie, R. Ayadi and A.J.M. Bakx for their input to this study; we thank C.C. Richardson for providing us the gp2.5-Δ21C samples from his lab.
Author contributions: J.C.-D., L X., M.T.J.H. and G.J.L.W. conceptualized the research; J.C.-D., and L.X. collected data; I.H. built the combined optical trapping and confocal microscope instrument and developed the MATLAB code for the analysis of kymograph data; S.A.S. and A.v.O. provided purified wild type T7 gp2.5 and tested their biochemical activity; S.-J.L. provided purified gp2.5-Δ21C and tested their biochemical activity; L.X. J.C.-D. and M.T.J.H. analyzed the data; J.C.-D., L.X., M.T.J.H. and G.J.L.W. wrote the manuscript; G.J.L.W. supervised the project; the manuscript is read, revised and confirmed by all the listed authors.

FUNDING

'Crowd management: the physics of genome processing in complex environments' of Stichting voor Fundamenteel Onderzoek der Materie, China Scholarship Council [201704910912]; European Union H2020 Marie-Sklowdowska Curie International Training Network Anti-Helix [859853]. Funding for open access charge: The general account of Gijs J.L. Wuite at Vrije Universiteit Amsterdam.

Conflict of interest statement. The combined optical tweezers and fluorescence technologies used in this article are patented and licensed to LUMICKS B.V., in which M.T.J.H., I.H., E.J.G.P. and G.J.L.W. declare financial interest. All other authors declare that they have no competing interests.

REFERENCES

1. Kim,Y.T. and Richardson,C.C. (1993) Bacteriophage T7 gene 2.5 protein: an essential protein for DNA replication. *Proc. Natl. Acad. Sci. U.S.A.*, **90**, 10173–10177.
2. Reuben,R.C. and Gefter,M.L. (1974) A Deoxyribonucleic Acid-Binding Protein Induced by Bacteriophage T7: PURIFICATION AND PROPERTIES OF THE PROTEIN. *J. Biol. Chem.*, **249**, 3843–3850.
3. Chase,J.W. and Williams,K.R. (1986) Single-stranded DNA binding proteins required for DNA replication. *Annu. Rev. Biochem.*, **55**, 103–136.
4. Kim,Y.T., Tabor,S., Bortner,C., Griffith,J.D. and Richardson,C.C. (1992) Purification and characterization of the bacteriophage T7 gene 2.5 protein. A single-stranded DNA-binding protein. *J. Biol. Chem.*, **267**, 15022–15031.
5. Lohman,T.M. and Ferrari,M.E. (1994) Escherichia coli single-stranded DNA-binding protein: multiple DNA-binding modes and cooperatives. *Annu. Rev. Biochem.*, **63**, 527–570.
6. Xu,L., Halma,M.T.J. and Wuite,G.J.L. (2023) Unravelling how single-stranded DNA binding protein coordinates DNA metabolism using single-molecule approaches. *Int. J. Mol. Sci.*, **24**, 2806.
7. Hollis,T., Stattel,J.M., Walther,D.S., Richardson,C.C. and Ellenberger,T. (2001) Structure of the gene 2.5 protein, a single-stranded DNA binding protein encoded by bacteriophage T7. *Proc. Nat. Acad. Sci. U.S.A.*, **98**, 9557–9562.
8. Hernandez,A.J. and Richardson,C.C. (2019) Gp2.5, the multifunctional bacteriophage T7 single-stranded DNA binding protein. *Semin. Cell Dev. Biol.*, **86**, 92–101.
9. Pant,K., Karpel,R.L., Rouzina,L. and Williams,M.C. (2004) Mechanical measurement of single-molecule binding rates: kinetics of DNA helix-destabilization by T4 gene 32 protein. *J. Mol. Biol.*, **336**, 851–870.
10. Shokri,L., Marintcheva,B., Richardson,C.C., Rouzina,I. and Williams,M.C. (2006) Single Molecule Force Spectroscopy of Salt-dependent Bacteriophage T7 Gene 2.5 Protein Binding to Single-stranded DNA. *J. Biol. Chem.*, **281**, 38689–38696.
11. Dubiel,K., Myers,A.R., Kozlov,A.G., Yang,O., Zhang,J., Ha,T., Lohman,T.M. and Keck,J.L. (2019) Structural mechanisms of cooperative DNA binding by bacterial single-stranded DNA-binding proteins. *J. Mol. Biol.*, **431**, 178–195.
12. Naufer,M.N., Morse,M., Möller,G.B., McIsaac,J., Rouzina,I., Beuning,P.J. and Williams,M.C. (2021) Multiprotein E. coli SSB–ssDNA complex shows both stable binding and rapid dissociation due to interprotein interactions. *Nucleic Acids Res.*, **49**, 1532–1549.
13. Suksombat,S., Khafizov,R., Kozlov,A.G., Lohman,T.M. and Chemla,Y.R. (2015) Structural dynamics of E. coli single-stranded DNA binding protein reveal DNA wrapping and unwrapping pathways. *Elife*, **4**, e08193.
14. Morin,J.A., Cerrón,F., Jarillo,J., Beltrán-Heredia,E., Ciesielski,G.L., Arias-Gonzalez,J.R., Kaguni,L.S., Cao,F.J. and Ibarra,B. (2017) DNA synthesis determines the binding mode of the human mitochondrial single-stranded DNA-binding protein. *Nucleic Acids Res.*, **45**, 7237–7248.
15. Honda,M., Park,J., Pugh,R.A. and Ha Taekjipand Spies,M. (2009) Single-molecule analysis reveals differential effect of ssDNA-binding proteins on DNA translocation by XPD helicase. *Mol. Cell*, **35**, 694–703.
16. Sokoloski,J.E., Kozlov,A.G., Galletto,R. and Lohman,T.M. (2016) Chemo-mechanical pushing of proteins along single-stranded DNA. *Proc. Natl. Acad. Sci. U.S.A.*, **113**, 6194–6199.
17. Cerrón,F., de Lorenzo,S., Lemishko,K.M., Ciesielski,G.L., Kaguni,L.S., Cao,F.J. and Ibarra,B. (2019) Replicative DNA polymerases promote active displacement of SSB proteins during lagging strand synthesis. *Nucleic Acids Res.*, **47**, 5723–5734.
18. Bhattacharyya,B., George,N.P., Thurmes,T.M., Zhou,R., Jani,N., Wessel,S.R., Sandler,S.J., Ha,T. and Keck,J.L. (2014) Structural mechanisms of PriA-mediated DNA replication restart. *Proc. Nat. Acad. Sci. U.S.A.*, **111**, 1373–1378.
19. Spenkelink,L.M., Lewis,J.S., Jergic,S., Xu,Z.-Q., Robinson,A., Dixon,N.E. and van Oijen,A.M. (2019) Recycling of single-stranded DNA-binding protein by the bacterial replisome. *Nucleic Acids Res.*, **47**, 4111–4123.
20. Ghosh,S., Hamdan,S. and Richardson,C. (2010) Two modes of interaction of the single-stranded DNA-binding protein of bacteriophage T7 with the DNA polymerase-thioredoxin complex. *J. Biol. Chem.*, **285**, 18103–18112.
21. Bull,J.J., Badgett,M.R., Rokyta,D. and Molineux,I.J. (2003) Experimental evolution yields hundreds of mutations in a functional viral genome. *J. Mol. Evol.*, **57**, 241–248.
22. Benkovic,S.J., Valentine,A.M. and Salinas,F. (2001) Replisome-mediated DNA replication. *Annu. Rev. Biochem.*, **70**, 181–208.
23. Hamdan,S.M., Marintcheva,B., Cook,T., Lee,S.-J., Tabor,S. and Richardson,C.C. (2005) A unique loop in T7 DNA polymerase mediates the binding of helicase-primase, DNA binding protein, and processivity factor. *Proc. Natl Acad. Sci. U.S.A.*, **102**, 5096–5101.
24. Matsumoto,T., Morimoto,Y., Shibata,N., Kinebuchi,T., Shimamoto,N., Tsukihara,T. and Yasuoka,N. (2000) Roles of functional loops and the CD-terminal segment of a single-stranded DNA binding protein elucidated by X-ray structure analysis. *The Journal of Biochemistry*, **127**, 329–335.
25. Cernooka,E., Rumnieks,J., Tars,K. and Kazaks,A. (2017) Structural basis for DNA recognition of a single-stranded DNA-binding protein from enterobacter phage Enc34. *Sci. Rep.*, **7**, 15529.
26. Bogutzki,A., Naue,N., Litz,L., Pich,A. and Curth,U. (2019) E. coli primase and DNA polymerase III holoenzyme are able to bind concurrently to a primed template during DNA replication. *Sci. Rep.*, **9**, 14460.
27. He,Z.-G. and Richardson,C.C. (2004) Effect of single-stranded DNA-binding proteins on the helicase and primase activities of the bacteriophage T7 gene 4 protein. *J. Biol. Chem.*, **279**, 22190–22197.
28. Kong,D. and Richardson,C.C. (1998) Role of the acidic carboxyl-terminal domain of the single-stranded DNA-binding protein of bacteriophage T7 in specific protein-protein interactions. *J. Biol. Chem.*, **273**, 6556–6564.
29. Kozlov,A.G., Weiland,E., Mittal,A., Waldman,V., Antony,E., Fazio,N., Pappu,R.V. and Lohman,T.M. (2015) Intrinsically disordered C-terminal tails of *E. coli* single stranded DNA binding protein regulate cooperative binding to single stranded DNA. *J. Mol. Biol.*, **427**, 763–774.
30. Tan,H.Y., Wilczek,L.A., Pottinger,S., Manosas,M., Yu,C., Nguyenduc,T. and Bianco,P.R. (2017) The intrinsically disordered linker of E. coli SSB is critical for the release from single-stranded DNA. *Protein Sci.*, **26**, 700–717.
31. Marintcheva,B., Marintchev,A., Wagner,G. and Richardson,C.C. (2008) Acidic C-terminal tail of the ssDNA-binding protein of bacteriophage T7 and ssDNA compete for the same binding surface. *Proc. Natl Acad. Sci. U.S.A.*, **105**, 1855–1860.
32. Kim,Y.T. and Richardson,C.C. (1994) Acidic carboxyl-terminal domain of gene 2.5 protein of bacteriophage T7 is essential for protein-protein interactions. *J. Biol. Chem.*, **269**, 5270–5278.
33. Hosoda,J. and Moise,H. (1978) Purification and physicochemical properties of limited proteolysis products of T4 helix destabilizing protein (gene 32 protein). *J. Biol. Chem.*, **253**, 7547–7558.
34. Williams,K.R., Spicer,E.K., LoPresti,M.B., Guggenheimer,R.A. and Chase,J.W. (1983) Limited proteolysis studies on the Escherichia coli single-stranded DNA binding protein. Evidence for a functionally homologous domain in both the Escherichia coli and T4 DNA binding proteins. *J. Biol. Chem.*, **258**, 3346–3355.
35. Hyland,E.M., Rezende,L.F. and Richardson,C.C. (2003) The DNA binding domain of the gene 2.5 single-stranded DNA-binding protein of bacteriophage T7. *J. Biol. Chem.*, **278**, 7247–7256.
36. Rezende,L., Willcox,S., Griffith,J. and Richardson,C. (2003) A single-stranded DNA-binding protein of bacteriophage T7 defective in DNA annealing. *J. Biol. Chem.*, **278**, 29098–29105.

37. Williams,K.R. and Konigsberg,W. (1978) Structural changes in the T4 gene 32 protein induced by DNA polynucleotides. *J. Biol. Chem.*, **253**, 2463–2470.
38. Candelli,A., Hoekstra,T.P., Farge,G., Gross,P., Peterman,E.J.G. and Wuite,G.J.L. (2013) A toolbox for generating single-stranded DNA in optical tweezers experiments. *Biopolymers*, **99**, 611–620.
39. Etson,C.M., Hamdan,S.M., Richardson,C.C. and Oijen,A.M.v. (2010) Thioredoxin suppresses microscopic hopping of T7 DNA polymerase on duplex DNA. *Proc. Natl. Acad. Sci. U.S.A.*, **107**, 1900–1905.
40. Heller,I., Sitters,G., Broekmans,O.D., Biebricher,A.S., Wuite,G.J.L. and Peterman,E.J.G. (2014) Mobility analysis of super-resolved proteins on optically stretched DNA: comparing imaging techniques and parameters. *ChemPhysChem*, **15**, 727–733.
41. Farge,G., Laurens,N., Broekmans,O.D., van den Wildenberg,S.M.J.L., Dekker,L.C.M., Gaspari,M., Gustafsson,C.M., Peterman,E.J.G., Falkenberg,M. and Wuite,G.J.L. (2012) Protein sliding and DNA denaturation are essential for DNA organization by human mitochondrial transcription factor A. *Nat. Commun.*, **3**, 1013.
42. Schmidt,T., Schütz,G.J., Baumgartner,W., Gruber,H.J. and Schindler,H. (1996) Imaging of single molecule diffusion. *Proc. Natl. Acad. Sci. U.S.A.*, **93**, 2926–2929.
43. Biebricher,A., Hirano,S., Enzlin,J.H., Wiechens,N., Streicher,W.W., Huttner,D., Wang,L.H.-C., Nigg,E.A., Owen-Hughes,T., Liu,Y. *et al.* (2013) PICH: a DNA translocase specially adapted for processing anaphase bridge DNA. *Mol. Cell*, **51**, 691–701.
44. Smith,S.B., Cui,Y. and Bustamante,C. (1996) Overstretching B-DNA: the elastic response of individual double-stranded and single-stranded DNA molecules. *Science*, **271**, 795–799.
45. Bosco,A., Camunas-Soler,J. and Ritort,F. (2014) Elastic properties and secondary structure formation of single-stranded DNA at monovalent and divalent salt conditions. *Nucleic Acids Res.*, **42**, 2064–2074.
46. Markham,N.R. and Zuker,M. (2008) UNAFold: software for nucleic acid folding and hybridization. *Methods Mol. Biol.*, **453**, 3–31.
47. Woodside,M.T., Behnke-Parks,W.M., Larizadeh,K., Travers,K., Herschlag,D. and Block,S.M. (2006) Nanomechanical measurements of the sequence-dependent folding landscapes of single nucleic acid hairpins. *Proc. Natl. Acad. Sci. U.S.A.*, **103**, 6190–6195.
48. Hatch,K., Danilowicz,C., Coljee,V. and Prentiss,M. (2007) Direct measurements of the stabilization of single-stranded DNA under tension by single-stranded binding proteins. *Phys. Rev. E*, **76**, 021916.
49. Morten,M.J., Peregrina,J.R., Figueira-Gonzalez Mariaand Ackermann,K., Bode,B.E., White,M.F. and Penedo,J.C. (2015) Binding dynamics of a monomeric SSB protein to DNA: a single-molecule multi-process approach. *Nucleic Acids Res.*, **43**, 10907–10924.
50. Ga,K., P,G., U,B., M,M., Gj,W. and Ej,P. (2013) Revealing the competition between peeled ssDNA, melting bubbles, and S-DNA during DNA overstretching using fluorescence microscopy. *Proc. Natl. Acad. Sci. U.S.A.*, **110**, 3859–3864.
51. Shokri,L., Marintcheva,B., Eldib,M., Hanke,A., Rouzina,I. and Williams,M.C. (2008) Kinetics and thermodynamics of salt-dependent T7 gene 2.5 protein binding to single- and double-stranded DNA. *Nucleic Acids Res.*, **36**, 5668–5677.
52. McGhee,J.D. and von Hippel,P.H. (1974) Theoretical aspects of DNA-protein interactions: co-operative and non-co-operative binding of large ligands to a one-dimensional homogeneous lattice. *J. Mol. Biol.*, **86**, 469–489.
53. Kowalczykowski,S.C., Paul,L.S., Lonberg,N., Newport,J.W., McSwiggen,J.A. and von Hippel,P.H. (1986) Cooperative and noncooperative binding of protein ligands to nucleic acid lattices: experimental approaches to the determination of thermodynamic parameters. *Biochemistry*, **25**, 1226–1240.
54. Zhou,R., Kozlov,A.G., Roy,R., Zhang,J., Korolev,S., Lohman,T.M. and Ha,T. (2011) SSB functions as a sliding platform that migrates on DNA via reptation. *Cell*, **146**, 222–232.
55. Shokri,L., Rouzina,I. and Williams,M.C. (2009) Interaction of bacteriophage T4 and T7 single-stranded DNA-binding proteins with DNA. *Phys. Biol.*, **6**, 025002.
56. Kowalczykowski,S.C., Lonberg,N., Newport,J.W., Paul,L.S. and von Hippel,P.H. (1980) On the thermodynamics and kinetics of the cooperative binding of bacteriophage T4-coded gene 32 (helix destabilizing) protein to nucleic acid lattices. *Biophys. J.*, **32**, 403–418.
57. Alani,E., Thresher,R., Griffith,J.D. and Kolodner,R.D. (1992) Characterization of DNA-binding and strand-exchange stimulation properties of y-RPA, a yeast single-strand-DNA-binding protein. *J. Mol. Biol.*, **227**, 54–71.
58. Kim,C., Paulus,B.F. and Wold,M.S. (1994) Interactions of human replication protein A with oligonucleotides. *Biochemistry*, **33**, 14197–14206.